Journal of Biomolecular NMR, **14:** 333–343, 1999.
KLUWER/ESCOM

TROSY-based HNCO pulse sequences for the measurement of ^{1}HN-^{15}N, ^{15}N-^{13}CO, ^{1}HN-^{13}CO, ^{13}CO-^{13}C$^{\alpha}$ and ^{1}HN-^{13}C$^{\alpha}$ dipolar couplings in ^{15}N, ^{13}C, ^{2}H-labeled proteins

Daiwen Yang, Ronald A. Venters, Geoffrey A. Mueller, W.Y. Choy & Lewis E. Kay
Protein Engineering Network Centres of Excellence and Departments of Medical Genetics, Biochemistry and Chemistry, University of Toronto, Toronto, ON, Canada M5S 1A8

Received 20 April 1999; Accepted 21 June 1999

Key words: alignment, deuterated proteins, dipolar couplings, HNCO, protein NMR, TROSY

Abstract

HNCO-based 3D pulse schemes are presented for measuring ^{1}HN-^{15}N,^{15}N-^{13}CO, ^{1}HN-^{13}CO,^{13}CO-^{13}C$^{\alpha}$ and ^{1}HN-^{13}C$^{\alpha}$ dipolar couplings in ^{15}N,^{13}C,^{2}H-labeled proteins. The experiments are based on recently developed TROSY methodology for improving spectral resolution and sensitivity. Data sets recorded on a complex of Val, Leu, Ile (δ1 only) methyl protonated ^{15}N,^{13}C,^{2}H-labeled maltose binding protein and β-cyclodextrin as well as ^{15}N,^{13}C,^{2}H-labeled human carbonic anhydrase II demonstrate that precise dipolar couplings can be obtained on proteins in the 30–40 kDa molecular weight range. These couplings will serve as powerful restraints for obtaining global folds of highly deuterated proteins.

Introduction

In the past several years a number of important methodological developments in high resolution NMR spectroscopy have led to significant increases in the size limitations that previously impeded solution structural studies of macromolecules. Specifically, the use of deuteration in concert with triple resonance pulse schemes with ^{2}H decoupling have facilitated backbone ^{1}HN,^{15}N, ^{13}C$^{\alpha}$ and side-chain ^{13}C$^{\beta}$ resonance assignment of proteins with correlation times (τ_C) on the order of 20–25 ns (Gardner and Kay, 1998). More recently, the development of TROSY triple resonance spectroscopy by Pervushin, Wüthrich and co-workers (1997, 1998a, b) has resulted in substantial sensitivity and resolution gains for applications to high molecular weight proteins. In this context we have demonstrated that 4D TROSY-triple resonance data sets with excellent sensitivity can be obtained for a complex of Val, Leu, Ile (δ1 only) methyl protonated ^{15}N,^{13}C,^{2}H-labeled maltose binding protein (MBP) and β-cyclodextrin having a correlation time of 46 ns at 5 °C (Yang and Kay, 1999b).

A second advance has been the development of anisotropic media for the alignment of macromolecules in solution with only a very modest decrease in spectral quality (Tjandra and Bax, 1997). This allows the measurement of dipolar couplings, providing a rich source of structural (Tjandra et al., 1997) and potentially dynamic (Tolman et al., 1997) information. This technology is of particular importance for large proteins and protein complexes where unambiguous interpretation of NOE cross peaks can be difficult (Zwahlen et al., 1998a, b). Moreover, many studies of large proteins are now performed on perdeuterated or specifically protonated, highly deuterated samples where the number of NOE restraints is dramatically reduced relative to those available from a fully protonated molecule. In these cases the additional information provided by dipolar couplings is essential to the calculation of accurate global folds.

Recently Bax and co-workers have described a simple 2D NMR experiment for the simultaneous measurement of ^{1}HN-^{15}N,^{15}N-^{13}CO and ^{1}HN-^{13}CO dipolar couplings in ^{15}N,^{13}C,^{2}H labeled proteins (Wang et al., 1998). In cases where resolution per-

mits, this approach allows recording of a large number of restraints very rapidly. In practice, however, measurement of dipolar couplings on large proteins is complicated by a number of factors. First, spectra are hampered by problems of resolution and sensitivity. Second, when measuring ^{1}HN-^{15}N dipolar couplings it is often observed that one of the components is severely attenuated from cross-correlated spin relaxation (Pervushin et al., 1997) resulting in significant measurement errors. With these problems in mind we have developed a suite of TROSY-HNCO-based 3D pulse schemes for measurement of one-bond ^{1}HN-^{15}N, ^{15}N-^{13}CO,^{13}CO-^{13}C$^{\alpha}$, two-bond ^{1}HN-^{13}CO and three-bond ^{1}HN-^{13}C$^{\alpha}$ couplings and demonstrate their utility on samples of ^{15}N,^{13}C,^{2}H-labeled human carbonic anhydrase (HCA II, 259 residues) and Val, Leu, Ile (δ1 only) methyl protonated ^{15}N,^{13}C,^{2}H-labeled maltose binding protein (MBP, 370 residues) complexed with β-cyclodextrin.

Materials and methods

^{15}N,^{13}C,^{2}H-HCA II and Val, Leu, Ile (δ1 only) methyl protonated ^{15}N,^{13}C,^{2}H-labeled MBP complexed with β-cyclodextrin were produced as described previously (Venters et al., 1996; Gardner et al., 1998). Samples were oriented using Pf1 phage, as described by Pardi and co-workers (Hansen et al., 1998). In the case of HCA II a concentration of phage of ≈11 mg/mL was used (^{2}H splitting of 10 Hz), while for MBP the phage concentration was ≈19 mg/mL (^{2}H splitting of 19 Hz). Sample conditions were: HCA II, 1.6 mM, 100 mM sodium phosphate, pH 6.8, 90% H_2O/10% D_2O, 30 °C; MBP, 1.4 mM/1.0 mM (no phage/phage), 2 mM β-cyclodextrin, 20 mM sodium phosphate (pH 7.2), 3 μM NaN_3, 100 μM EDTA, 0.1 mg/mL Pefabloc, 1 μg/μL pepstatin, 90% H_2O/10% D_2O, 37 °C. HCA II and MBP data were recorded on Varian Inova 500 and 600 MHz spectrometers, respectively. Similar acquisition and processing parameters were employed for both HCA II and MBP data sets; only values for MBP will be reported here. All of the data sets were processed with NMRPipe software (Delaglio et al., 1995) and analyzed with the PIPP/CAPP (Garrett et al., 1991) routines.

Measurement of one-bond ^{1}HN-^{15}N couplings: Data matrices comprising 34, 39, 1152 complex points in each of (t_1,t_2,t_3) were acquired corresponding to acquisition times of (21.8 ms, 23.8 ms, 128 ms). For each measurement of $^{1}J_{NH}$ two experiments were recorded (schemes iii and iv of Figure 1), with a net acquisition time of 10.5 h/experiment for the unoriented sample and 21 h/experiment in the case of alignment. The ^{15}N time domain was doubled with mirror image linear prediction (Zhu and Bax, 1990) in the case of scheme iii ($\kappa = 0$) and with forwards-backwards linear prediction (Zhu and Bax, 1992) for scheme iv ($\kappa = 2$). Final data sets comprised (128, 512, 797) real points corresponding to (11.8 Hz/pt, 3.1 Hz/pt, 3.9 Hz/pt) in each of (F_1,F_2,F_3).

Measurement of one-bond ^{15}N-^{13}CO and two-bond ^{1}HN-^{13}CO couplings: Data sets of (34, 48, 1152) complex points and acquisition times of (21.8 ms, 29.4 ms, 128 ms) were obtained in measuring times of 24 and 48 h for spectra recorded in the absence and presence of phage. A value of $\kappa = 4$ was used in all cases. The t_1 time domain was doubled with forwards-backwards linear prediction. Final data sets of (128, 512, 1418) points were generated, with (11.8 Hz/pt, 3.1 Hz/pt, 2.2 Hz/pt) in each of (F_1,F_2,F_3).

Measurement of one-bond ^{13}CO-^{13}C$^{\alpha}$ and three-bond ^{1}HN-^{13}C$^{\alpha}$ couplings: Matrices comprising (74, 40, 1152) complex points and (t_1,t_2,t_3) acquisition times of (44.2 ms, 24.4 ms, 128 ms) were recorded. Measuring times of 22 and 43 h were used for 3D spectra recorded without and with phage, respectively. The ^{15}N time domain was doubled with mirror image linear prediction to give a final data set of (512, 128, 1418) points corresponding to a digital resolution of (3.22 Hz/pt, 12.5 Hz/pt, 2.2 Hz/pt) in each of (F_1,F_2,F_3).

Results and discussion

Figure 1 illustrates the HNCO pulse schemes that have been employed to measure the one-bond ^{1}HN-^{15}N (A), one-bond ^{15}N-^{13}CO, two-bond ^{1}HN-^{13}CO (B) and one-bond ^{13}CO-^{13}C$^{\alpha}$, three-bond ^{1}HN-^{13}C$^{\alpha}$ (C) dipolar couplings using the TROSY principle in the ^{15}N and ^{1}HN dimensions. It is noteworthy that our implementation (Yang and Kay, 1999a,b) differs from the approach originally developed by Pervushin et al. (1998a) in the transfer of magnetization from ^{15}N to ^{1}HN prior to detection. For applications to proteins with correlation times in excess of ≈ 20 ns sensitivity gains can be realized using this approach since magnetization is placed along the Z-axis for parts of

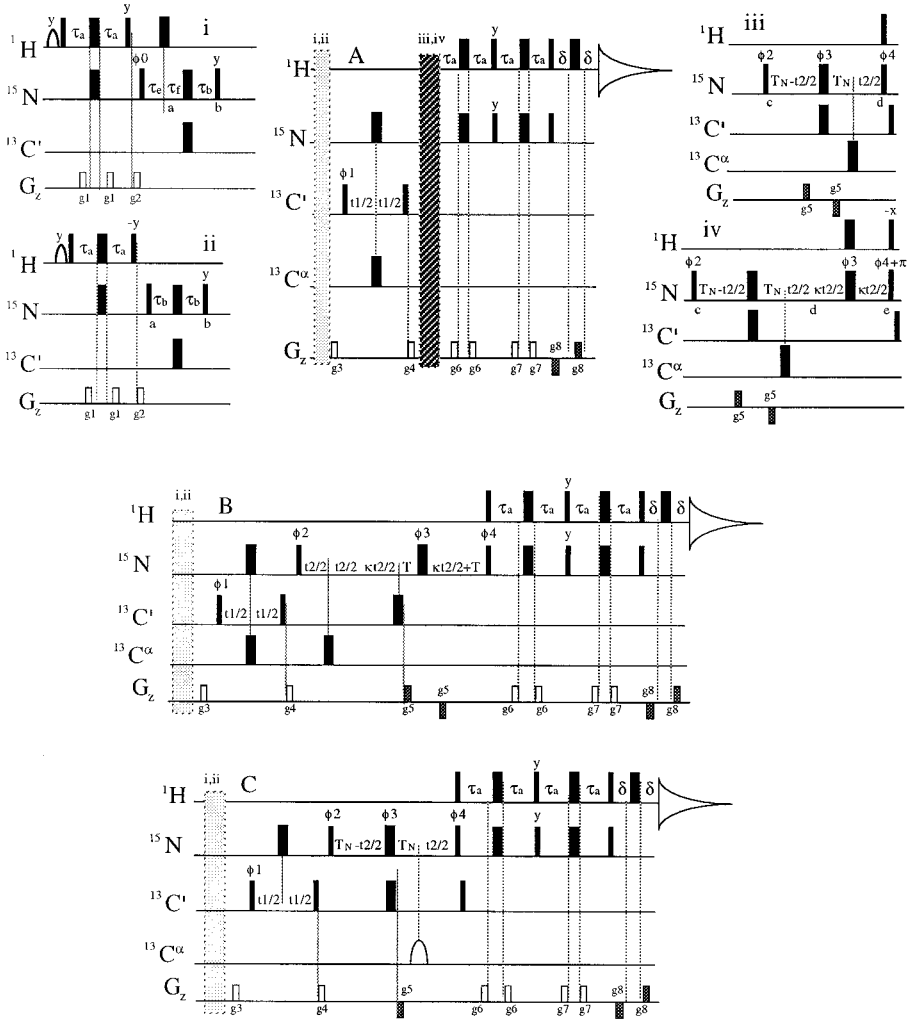

Figure 1. HNCO, TROSY-based pulse schemes used to measure ^{1}HN(i)–^{15}N(i) (A), ^{15}N(i)–^{13}CO(i-1), ^{1}HN(i)–^{13}CO(i-1) (B), and ^{13}CO(i-1)–^{13}C$^\alpha$(i-1), ^{1}HN(i)–^{13}C$^\alpha$(i-1) (C) dipolar couplings in ^{15}N,^{13}C,^{2}H-labeled proteins. Schemes (i) or (ii) are inserted in the light shaded rectangle in experiments A–C, depending on whether active suppression of the anti-TROSY component is desired (scheme i). All narrow (wide) pulses are applied with a flip angle of 90° (180°) with the phase indicated above each pulse if it is different from x. The phases have been verified for Varian spectrometers. ^{1}H, ^{13}C and ^{15}N carriers are centered at the water line, 176 and 119 ppm, respectively. ^{1}H and ^{15}N pulses are applied with field strengths of 31 and 6.25 kHz, respectively, with the exception of the shaped water selective 90° pulse at the start of the sequences which has the EBURP-1 profile (7 ms) (Geen and Freeman, 1991). All ^{13}C rectangular 90° (180°) pulses are applied with a field strength of $\Delta/\sqrt{15}$ ($\Delta/\sqrt{3}$), where Δ is the separation in Hz between the centers of the ^{13}C$^\alpha$ and ^{13}CO chemical shift regions (Kay et al., 1990). The shaped ^{13}C$^\alpha$ pulse of sequence C has a g3 profile (500 μs at 600 MHz) (Emsley and Bodenhausen, 1987). All ^{13}C$^\alpha$ pulses are generated by phase modulation of the carrier (Boyd and Scoffe, 1989; Patt, 1992). The delays used are: τ_a = 2.3 ms, τ_b = 12.4 ms, τ_e = 1.34 ms, $\tau_f = \tau_b - \tau_e$, T$_N$ = 12.4–13 ms, T = 700 μs and δ = 250 μs. The phase cycle employed is: ϕ0 = 45°; ϕ1 = 2(x),2(−x); ϕ2 = (y,−y) for sequences A and C, (x,−x) for B; ϕ3 = 2(x),2(−x); ϕ4 = x; rec = x,2(−x), x. Note that the value of ϕ0 must be adjusted carefully to minimize the anti-TROSY component. This is achieved using sequence A, with schemes i and iii by moving the ^{1}H 180° pulse at point a in scheme i immediately before the ^{15}N pulse of phase ϕ0 and adjusting ϕ0 for a null. The ϕ0 that is to be used in the actual experiment is 1/2 the value at which a null is obtained. The phases of the second ^{1}H 90° pulse (labeled y and −y in scheme i and ii, respectively) and the water selective pulse must be inverted for applications on Bruker spectrometers (Zhu et al., 1999). Quadrature detection in F$_1$ is achieved via States-TPPI of ϕ1 (Marion et al., 1989), while quadrature detection in the ^{15}N dimension employs the gradient enhanced sensitivity method where for each t$_2$ value the phase ϕ4 is incremented by 180° and the sign of g5 inverted (Kay et al., 1992; Schleucher et al., 1993). 180° is added to the phase ϕ2 and to the phase of the receiver for each complex t$_2$ point (Marion et al., 1989). The gradients used are: g1 = (0.5 ms, 5 G/cm), g2 = (1 ms, 15 G/cm), g3 = (0.75 ms, 10 G/cm), g4 = (0.5 ms, 10 G/cm), g5 = (0.625 ms, 30 G/cm) for A and B and (1.25 ms, 30 G/cm) for C, g6 = (0.4 ms, 3.6 G/cm), g7 = (0.4 ms, 5.2 G/cm), g8 = (62.5 μs, 28.75 G/cm). In sequence A the dark shaded region is to be replaced with scheme iii ($\kappa = 0$) or scheme iv ($\kappa \neq 0$).

the transfer (Yang and Kay, 1999a). As described in detail previously, suppression of the undesired multiplet (anti-TROSY) component associated with each (^{15}N,^{1}HN) correlation and arising from the transfer $N_{TR}(1 + 2\ HN_z) \rightarrow HN_{TR}(1 - 2N_z)$ occurs through relaxation during the relatively long periods where ^{15}N magnetization resides in the transverse plane (X_{TR} and X_z are transverse and Z components of magnetization, respectively). Active suppression of this component can also be achieved during the transfer of magnetization from ^{15}N to ^{13}CO using a scheme in which the two components, $N_{TR}(1\pm 2HN_z)$, are allowed to evolve until they are 90 ° out of phase, with the undesired signal subsequently purged. This has been discussed originally by Pervushin et al. (1998b) in connection with ^{13}C-^{1}H correlated spectroscopy of aromatic groups in proteins and more recently in the context of our implementation of triple resonance TROSY (Yang and Kay, 1999b) (see supplementary material of this reference). If possible, active suppression should be avoided, however, as magnetization that contributes to the signal of interest does in fact originate on the fast relaxing ^{15}N component where it remains for the first $1/(8J_{NH})$ of the ^{15}N $\rightarrow$^{13}CO transfer period (J_{NH} is the one-bond ^{15}N-^{1}HN scalar coupling constant). Because all of the experiments described in this manuscript were recorded at field strengths of either 500 (HCA II, $\tau_C = 11$ ns at 30 °C) or 600 MHz (MBP, $\tau_C = 17$ ns at 37 °C), where maximal ratios of TROSY/anti-TROSY components of no more than 12/1 are predicted on the basis of relaxation alone, we have employed the sequences illustrated in scheme i of Figure 1 with active suppression. For applications to large proteins at higher fields, it is possible to remove the purging element as illustrated in scheme ii.

Since all of the experiments of Figure 1 are based on the TROSY-HNCO pulse sequence which has been described in some detail previously (Yang and Kay, 1999a), only a brief description of each experiment is provided with features important for recording each of the dipolar couplings highlighted. The magnetization pathway for all of the sequences can be described as,

$$\begin{aligned} &^{1}\mathrm{HN} \xrightarrow{^{1}\boldsymbol{J}_{\mathrm{NH}}} {}^{15}\mathrm{N} \xrightarrow{^{1}\boldsymbol{J}_{\mathrm{N,CO}}} \\ &{}^{13}\mathrm{CO}\ (t_1) \xrightarrow{^{1}\boldsymbol{J}_{\mathrm{N,CO}}} {}^{15}N\ (t_2) \xrightarrow{^{1}\boldsymbol{J}_{\mathrm{NH}}} {}^{1}\mathrm{HN}(t_3) \end{aligned} \qquad (1)$$

with the active couplings (dipolar + scalar) for transfer between different nuclei listed above each arrow. In the description that follows we will use the bold-faced $\boldsymbol{J}_{ij}$ to denote the sum of dipolar, D_{ij}, and scalar, J_{ij}, contributions.

Measurement of ^{1}HN-^{15}N dipolar couplings is achieved using sequence A, by recording two spectra with different κ values. Cross peaks are observed at the coordinates $(\omega_{CO} - \pi^{2}\boldsymbol{J}_{HN,CO}, \omega_N - (\kappa + 1)\pi^{1}\boldsymbol{J}_{NH}, \omega_{HN} + \pi^{1}\boldsymbol{J}_{NH}),^{1}\boldsymbol{J}_{NH} < 0$. Typically spectra are recorded with $\kappa = 0$ (scheme iii) and $\kappa = 2$ (scheme iv) so that a particular cross peak is shifted between spectra by $^{1}\boldsymbol{J}_{NH}$ Hz in the ^{15}N dimension. By recording a set of spectra with and without molecular alignment and noting that the sign of the scalar coupling contribution to $^{1}\boldsymbol{J}_{NH}$ is negative, the value of the ^{1}HN-^{15}N dipolar coupling, $^{1}D_{NH}$, can be obtained directly. It is noteworthy that although TROSY is operative during intervals extending from a to b and from c to d in the sequence, during the period from d to e transverse relaxation proceeds with an effective rate that is given by the average of the rates of the individual ^{15}N multiplet components. This limits the optimal value of κ for large molecules. In practice we find that a value of $\kappa = 2$ represents a good compromise between sensitivity requirements (which decrease with κ) and separation of cross peaks between spectra (which increases with κ). In the case of MBP at 37 °C, for example, a sensitivity decrease of a factor of ≈ 2 was measured between the $\kappa = 0$ and $\kappa = 2$ spectra. In cases where sensitivity is limiting it may be advantageous to record spectra with and without a ^{1}H 180 ° pulse immediately prior to the final $t_2/2$ period during the constant time ^{15}N evolution interval using scheme iii. (Note that in the case where a ^{1}H 180 ° pulse is added, the phase of the subsequent ^{1}H 90 ° must be inverted to ensure selection of the TROSY component.) In this case cross peaks are separated by $^{1}J_{NH}/2$ Hz between spectra, doubling the error of measurement. For this reason we prefer the scheme where values of $\kappa = 0, 2$ are used.

A point of interest regarding this sequence concerns the inclusion of a ^{13}CO 90 ° purge pulse after the ^{15}N pulse of phase φ4 (iii) or φ4 + π (iv). In cases where $2T_N < 1/(2^{1}J_{N,CO})$ this pulse is essential to ensure pure absorptive lineshapes in F_2 and F_3. It can be shown that in spectra recorded without this pulse the time domain signal arising from the evolution of $HN_y(1+2N_z)$ during t_3 is given by,

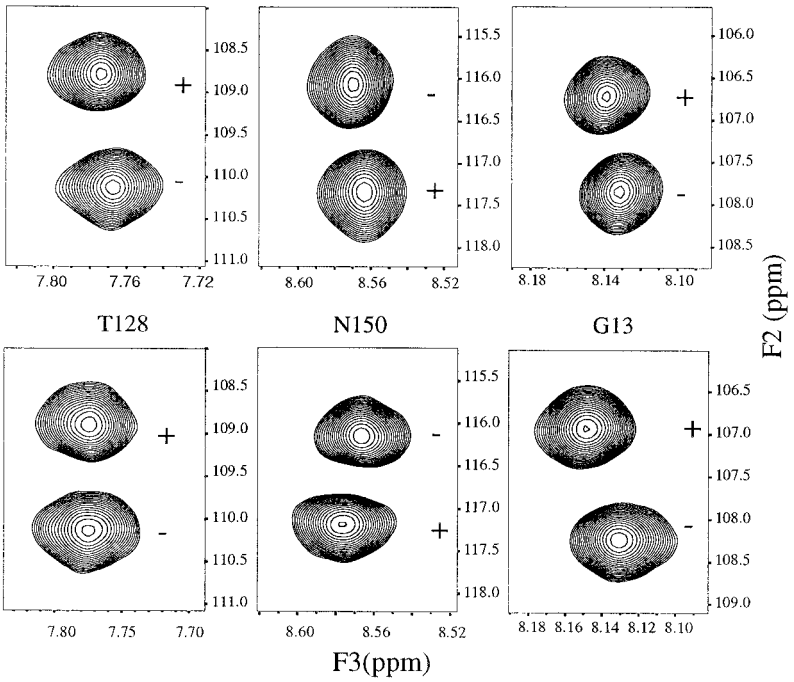

Figure 2. Selected regions from spectra recorded at 600 MHz on MBP with sequence 1B. The splittings in F_2 and F_3 provide a measure of $^1J_{N,CO}$ and $^2J_{HN,CO}$, respectively. The upper panels are from spectra of the protein in isotropic media, while the bottom traces are from spectra recorded with the protein aligned with phage. The phases of the multiplet components are indicated by $+/-$. Note that the multiplet phases are inverted for N150 relative to the other traces. This arises from the fact that the crosspeak for N150 is aliased in the ^{13}CO dimension where the first time point is set to half the dwell.

$$\begin{aligned}
&\cos(\omega_{CO} - \pi^2 J_{HN,CO})t_1 \\
&\times\{-\sin(2\pi^1 J_{N,CO} T_N)\cos(\omega_N - \pi^1 J_{NH})t_2 \\
&\cos(\omega_{HN} + \pi^1 J_{NH})t_3 \cos(\pi^2 J_{HN,CO} t_3) \qquad (2)\\
&+\cos(2\pi^1 J_{N,CO} T_N)\sin(\omega_N - \pi^1 J_{NH})t_2 \\
&\sin(\omega_{HN} + \pi^1 J_{NH})t_3 \sin(\pi^2 J_{HN,CO} t_3)\},
\end{aligned}$$

where all multiplicative factors, including those associated with relaxation, have been neglected, $\kappa = 0$, $\phi 1 = x$ and $\phi 2 = y$. For most applications involving large proteins the value of $2T_N$ is chosen to be somewhat less than $1/(2^1 J_{N,CO})$, so that $\cos(2\pi^1 J_{N,CO} T_N) \neq 0$. In cases where $2T_N < 1/(2^1 J_{N,CO})$ and $^2J_{HN,CO} \neq 0$, Equation 2 predicts and experiment verifies that the F_2/F_3 lineshapes are not purely absorptive. We have measured $^2J_{HN,CO}$ (see below) and in the absence of orientation an average value of $+4.4 \pm 0.4$ Hz for MBP is obtained. In the case of oriented MBP, values of $^2J_{HN,CO}$ vary between -10 and 8 Hz. This gives rise to a peakshape resembling what might be observed for cross peaks in E.COSY spectra (Griesinger et al., 1986) where the multiplet components in either of F_2/F_3 are not well resolved, with the skew of the peak depending on the sign of $^2J_{HN,CO}$. Since the second term of Equation 2 arises from nitrogen magnetization that is antiphase with respect to the one-bond coupled CO spin at the end of the $2T_N$ period, the CO purge pulse (and the subsequent action of gradient pulses) eliminates the antiphase contribution completely.

As noted above we have used scheme i in conjunction with all of the experiments to ensure that the fast relaxing multiplet component is completely eliminated. In the case of unoriented samples where $^1J_{NH} = ^1 J_{NH} \approx -94$ Hz, it is possible to adjust the value of τ_e to ensure proper elimination of the undesired component [$\tau_e = 1/(8^1 J_{NH})$]. In contrast, alignment results in a non-uniform distribution of $^1J_{NH}$ values and a single value of τ_e will not be optimal for all residues. In this case a value of τ_e set to $1/(8^1 J_{NH})$ results in intensities of $\cos\{\pi/4(1 - ^1 J_{NH}/^1 J_{NH})\}$ and $\sin\{\pi/4(1 - ^1 J_{NH}/^1 J_{NH})\}$ for the TROSY and anti-TROSY components, respectively. For the largest value of $^1D_{NH} \approx 30$ Hz obtained for MBP, the cosine and sine terms are 0.97 and 0.25, respectively,

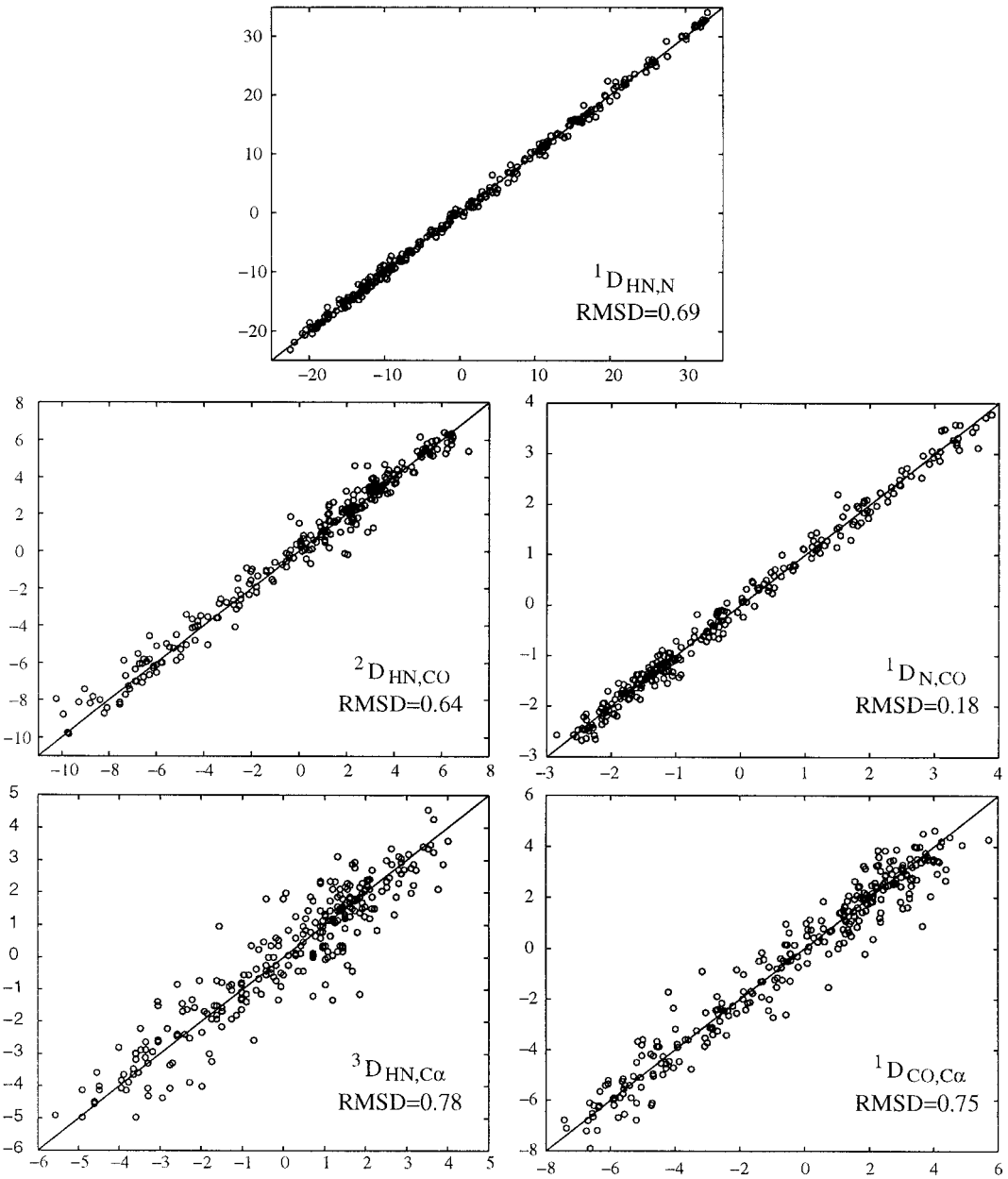

Figure 3. Correlations between D_{ij} values measured from repeat experiments on MBP. The pair-wise rmsd values obtained are indicated in the lower right hand corner of each plot.

and little intensity is lost from the desired correlations (< 3%). For non-extreme values of $^1D_{NH}$ the cosine and sine terms are closer to 1 and 0, respectively, and significantly less than 3% of the TROSY signal is lost while better suppression is achieved. Nevertheless, the minimal factor of 4 suppression from the purging in combination with attenuation due to relaxation is sufficient to eliminate the non-desired component for both HCA II and MBP data sets.

Figure 1B shows the E.COSY-based TROSY-HNCO sequence used to measure $^1D_{N,CO}$ and $^2D_{HN,CO}$. The time domain signal derived from the y component of ^{1}HN magnetization is proportional to

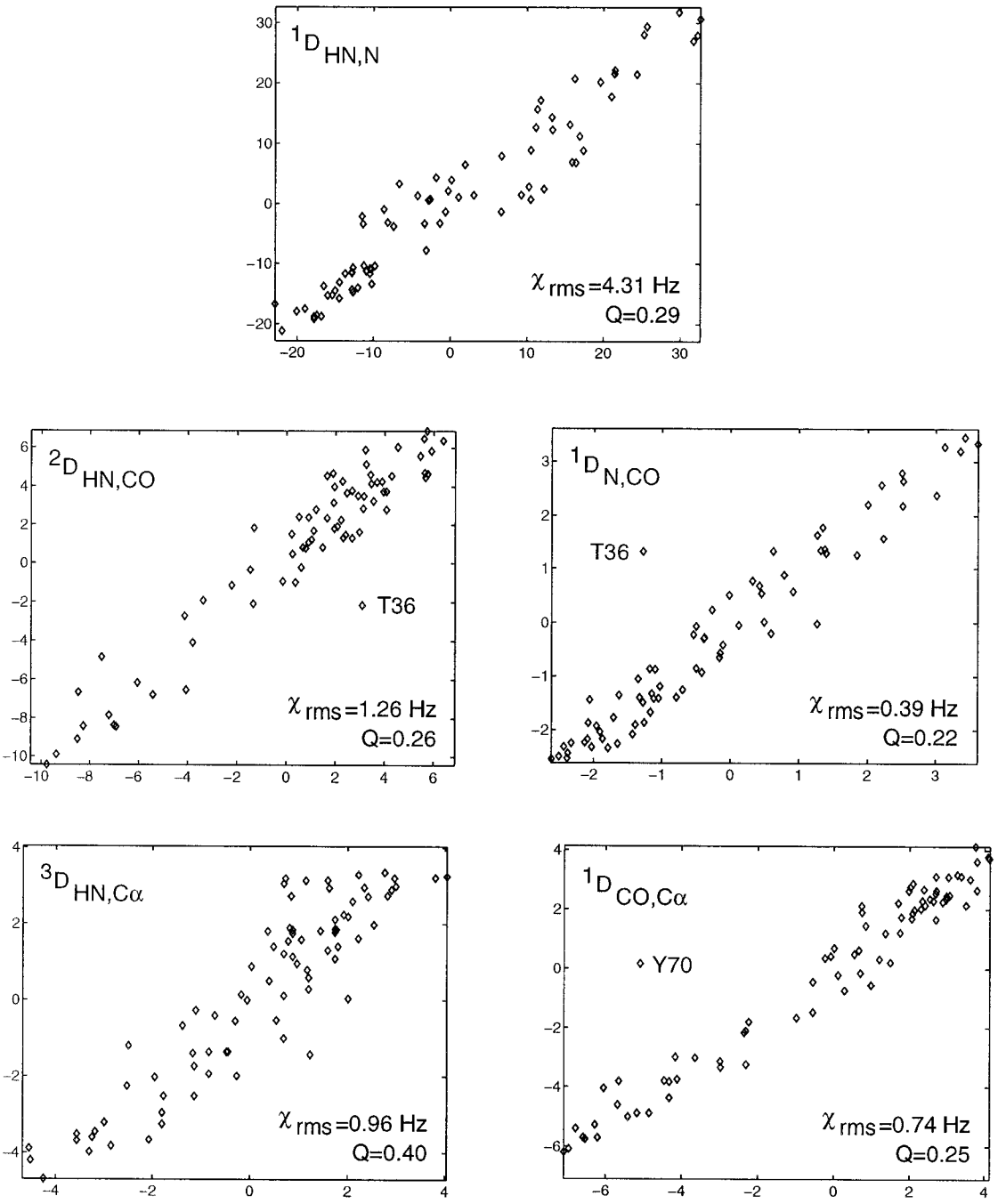

Figure 4. Comparison between measured D_{ij} couplings from regular secondary structural elements in the N-terminal domain of MPB complexed with β-cyclodextrin with values predicted on the basis of the X-ray structure of the complex (Sharff et al., 1993). Values of the axial (A_a) and rhombic (R) components of the alignment tensor of 0.00152 and 0.203 were obtained for the N domain from a best fit to all couplings by minimization of the difference between measured and predicted dipolar couplings. Euler angles (α,β,γ) = (104°,28°,31°) describe the orientation of the alignment frame in the X-ray coordinate system. Outliers are indicated by residue number and have been excluded from the calculations of χ_{rms} and $Q = \chi_{rms}/{}^1D_{rms}$ (${}^1D_{rms} = \{D_a^2[4 + 3(D_r/D_a)^2]/5\}^{0.5}$). Very similar values of Q were obtained when ${}^1D_{rms}$ was calculated from the rms experimental values. The N-terminal domain comprises residues 1–109, 264–309; residues 17–29, 42–49, 64–72, 83–87, 91–93, 273–281, 288–294 are in helices, while residues 6–11, 34–39, 58–62, 76–81, 102–109, 264–266, 301–303 are in β-strands as established by the CSI (Wishart and Sykes, 1994). A_a and R values of 0.00144 and 0.185 were obtained for the C-terminal domain of MBP. Effective internuclear distances were taken from Ottiger and Bax (1998); an inter-residue HN-Cα distance of 2.56 Å was used along with an S value of 0.95 for the HN-Cα dipolar interaction.

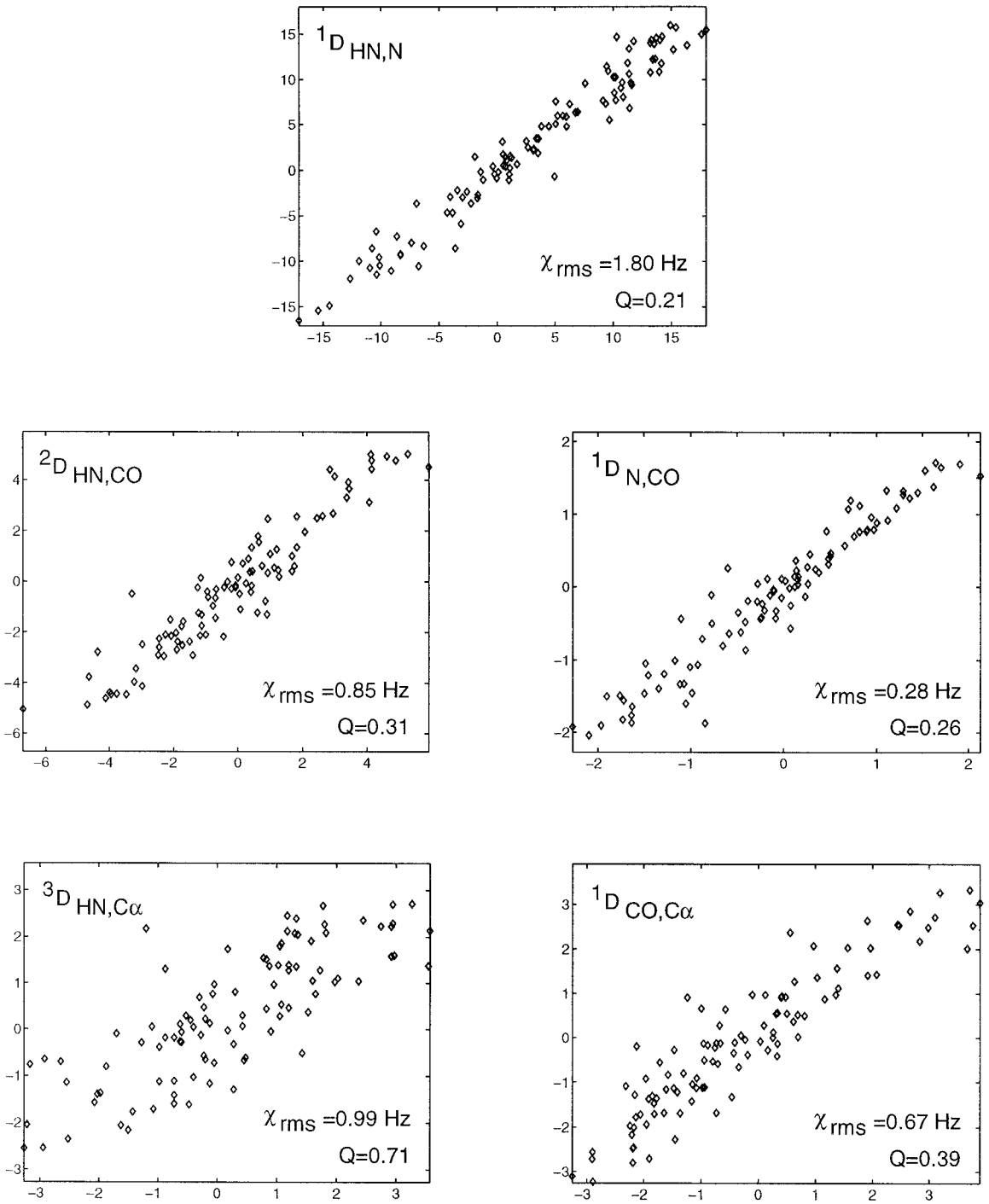

Figure 5. Comparison of measured and X-ray predicted (Hakansson et al., 1992) D_{ij} couplings from HCA II, including only elements of regular secondary structure. Values of the axial and rhombic components of the alignment tensor of −0.00080 and 0.603 where obtained; Euler angles of $(\alpha,\beta,\gamma) = (126°,109°,66°)$ describe the transformation from the X-ray coordinate system to the alignment frame. Residues in elements of secondary structure include: 13–18, 21–24, 125–127, 129–133, 154–166, 180–183, 219–225 in helices and 31–33, 38–40, 45–50, 55–61, 65–71, 77–81, 87–98, 108–109, 116–124, 139–150, 172–175, 189–195, 204–211, 214–217, 255–258 in β-strands.

$$\cos(\omega_{CO} - \pi^2 J_{HN,CO})t_1$$
$$\times\{\cos(\omega_N - \pi^1 J_{NH} + (1+\kappa)\pi^1 J_{N,CO})t_2$$
$$\cos(\omega_{HN} + \pi^1 J_{NH} - \pi^2 J_{HN,CO})t_3 \quad (3)$$
$$-\cos(\omega_N - \pi^1 J_{NH} - (1+\kappa)\pi^1 J_{N,CO})t_2$$
$$\cos(\omega_{HN} + \pi^1 J_{NH} + \pi^2 J_{HN,CO})t_3\}$$

where multiplicative factors have been omitted and $\phi 1 = \phi 2 = x$ in the sequence. Cross-peaks are observed at (F_1, F_2, F_3) = ($\omega_{CO} - \pi^2 J_{HN,CO}$, $\omega_N - \pi^1 J_{NH} + (1+\kappa)\pi^1 J_{N,CO}$, $\omega_{HN} + \pi^1 J_{NH} - \pi^2 J_{HN,CO}$) and ($\omega_{CO} - \pi^2 J_{HN,CO}$, $\omega_N - \pi^1 J_{NH} - (1+\kappa)\pi^1 J_{N,CO}$, $\omega_{HN} + \pi^1 J_{NH} + \pi^2 J_{HN,CO}$). The E.COSY cross-peaks, separated by $|(1+\kappa)^1 J_{N,CO}|$ and $|^2 J_{HN,CO}|$ Hz in F_2 and F_3, respectively, are of opposite phase and therefore there is no signal at $t_2 = t_3 = 0$. Signal does evolve as a function of t_3, however (even for $t_2 = 0$), due to the finite $^2 J_{HN,CO}$ value. Values of $^1D_{N,CO}$ and $^2D_{HN,CO}$ are measured by recording spectra in both isotropic and aligning media with the correct sign of each coupling obtained by noting that the scalar couplings, $^1J_{N,CO}$ and $^2J_{HN,CO}$ (i.e., isotropic solution) are negative and positive, respectively (Delaglio et al., 1991).

Figure 1C illustrates the E.COSY pulse scheme for measuring $^1D_{CO,C\alpha}$ and $^3D_{HN,C\alpha}$ couplings. Correlations at frequencies of (ω_1,ω_2,ω_3) = ($\omega_{CO} \pm \pi^1 J_{CO,C\alpha} - \pi^2 J_{HN,CO}$, $\omega_N - \pi^1 J_{NH}$, $\omega_{HN} + \pi^1 J_{NH} \mp \pi^3 J_{HN,C\alpha}$) are obtained, with $^1 J_{CO,C\alpha}$ determined directly from the displacement of multiplet components in F_1. (Evolution due to $^2J_{HN,CO}$ during t_3 has been ignored.) It is noteworthy that the multiplet component which is displaced by $^1 J_{CO,C\alpha}/2$ Hz in F_1 is also displaced by $-^3 J_{HN,C\alpha}/2$ Hz in F_3, while the second component is displaced by $-^1 J_{CO,C\alpha}/2$ Hz and $^3 J_{HN,C\alpha}/2$ Hz in F_1 and F_3, respectively. The opposite signs originate from the $^{13}C^\alpha$ 180° pulse applied between the ^{13}CO (t_1) and ^1HN (t_3) evolution periods. Thus, if the slope of the line connecting the two E.COSY multiplet components is positive (negative), $^1 J_{CO,C\alpha} \times^3 J_{HN,C\alpha}$ is negative (positive) and since $^1 J_{CO,C\alpha} > 0$, $^3 J_{HN,C\alpha} < 0$ (>0).

Unlike the previous sequences, where accordion spectroscopy (Bodenhausen and Ernst, 1981) has been used to extend the ^{15}N evolution period during which the relevant J coupling evolves ($^1 J_{NH}$ or $^1 J_{N,CO}$), in the present experiment the ^{13}CO chemical shift and the $^1 J_{CO,C\alpha}$ coupling are recorded for the same net duration, t_1. The large magnitude of the $^1 J_{CO,C\alpha}$ coupling and the relatively fast relaxation of the ^{13}CO spin (compared to the slow relaxing TROSY ^{15}N component, for example) limit the utility of the accordion approach for the measurement of $^1 J_{CO,C\alpha}$. Finally, a ^{13}CO 90° purge pulse is applied after the ^{15}N t_2 evolution period to eliminate dispersive contributions to cross-peak lineshapes in the F_2/F_3 dimensions, as described in the context of the scheme of Figure 1A.

Figure 2 illustrates a number of F_2/F_3 slices from data sets obtained with the sequence of Figure 1B for measuring $^1D_{N,CO}$ and $^2D_{HN,CO}$. The upper three traces are from an unoriented MBP sample, with the corresponding correlations from the aligned sample shown at the bottom. The value of $^1 J_{N,CO}$ is measured from the difference in splitting in F_2 (difference/[1 + κ]) and is negative for all residues of MBP in isotropic solution. With alignment, values of $^1 J_{N,CO}$ and $^2 J_{HN,CO}$ change considerably, with $^2 J_{HN,CO}$ inverting sign in the case of N150. The magnitude of $^2 J_{HN,CO}$ is recorded from the displacement along F_3, noting that if the slope of the line connecting the components is negative the value of $^2 J_{HN,CO}$ is positive. This can be understood by noting that the value of the scalar coupling $^2J_{HN,CO}$ is positive (Delaglio et al., 1991) and that the slope of the line connecting the components in spectra recorded without alignment is negative. The slope is opposite in sign to what Bax and co-workers observed in 2D E.COSY-based experiments (Delaglio et al., 1991). The difference arises from the fact that in the present experiment (sequence 1B) ^{15}N chemical shift evolution proceeds for a time of $-t_2$, while evolution due to $^1 J_{N,CO}$ occurs for a period of $(1 + \kappa)t_2$. In contrast, in the experiment of Delaglio et al. ^{15}N evolution due to chemical shift and $^1 J_{N,CO}$ proceeds for $+t_2$.

Figure 2 emphasizes the substantial linewidths of the multiplet components in relation to their separation, suggesting the possibility of systematic errors in measurement of $^1 J_{N,CO}$ and $^2 J_{HN,CO}$ values. The effects of finite multiplet linewidths on the measured values of $^1D_{N,CO}$ and $^2D_{HN,CO}$ for various κ values using experimental acquisition and processing parameters (75° shifted sine-bell squared window functions) have been simulated from synthetic data generated using the simTimeND routine in NMRDraw. ^{15}N and ^1HN transverse relaxation times for the TROSY component of 70 and 30 ms, respectively, were used. For a κ value of 4, employed in all experiments, and for -3 Hz $\leq {}^1D_{N,CO} \leq 4$ Hz and $|^2D_{HN,CO}| \leq 8.8$ Hz (corresponding to the range of values observed experimentally for MBP) $^1D_{N,CO}$ can be underestimated by

as much as 0.3 Hz, with the largest errors occurring when $^1D_{N,CO}$ is 4 Hz ($^1J_{N,CO} \approx -11$ Hz). Errors in $^2D_{HN,CO}$ are less than 0.4 Hz. For values of $\kappa < 4$ errors in dipolar couplings exceeding 1 Hz can be obtained in certain pathological cases.

Simulations have also been performed to establish the errors in measured $^1D_{CO,C\alpha}$ and $^3D_{HN,C\alpha}$ couplings. For values of $|^1D_{CO,C\alpha}| \leq 7$ Hz and $|^3D_{HN,C\alpha}| \leq 4.4$ Hz and assuming ^{13}CO T_2 values of 30 and 21 ms for the downfield and upfield multiplet components ($\omega_{CO} \pm \pi^1 J_{CO,C\alpha}$), values of $^1D_{CO,C\alpha}$ and $^3D_{HN,C\alpha}$ can be in error by as much as 0.5 Hz and 0.2 Hz, respectively.

The reproducibility of the experiments and contributions from random errors were evaluated by recording each data set twice. Figure 3 shows the correlation between dipolar couplings measured from duplicate experiments recorded on $\approx$ 1 mM MBP samples (with and without phage). The agreement between repeat experiments is reasonably good, as indicated by the pairwise rmsd values in the figure. Average values for ($^1J_{NH}$, $^1J_{N,CO}$, $^2J_{HN,CO}$,$^1J_{CO,C\alpha}$, $^3J_{HN,C\alpha}$) measured in the unoriented MBP sample are (-93.7 ± 1.1, -15.3 ± 0.8, 4.4 ± 0.4, 52.5 ± 1.0, 0.3 ± 0.4) Hz based on values from $\approx$ 275 well-resolved correlations in the spectra. $^1D_{NH}$ values have also been measured from 2D ^{1}HN-^{15}N spectra of MBP recorded with the IPAP method (Yang and Nagayama, 1996; Ottiger et al., 1998). A pair-wise rmsd of 1.0 Hz was obtained between values measured using this approach and the method of Figure 1A (75 residues were sufficiently well resolved in the 2D data sets to be included in the comparison), with no indication of any systematic differences between the two methods.

Figures 4 and 5 show comparisons between predicted D_{ij} values, calculated from the X-ray structures, and measured D_{ij} couplings for residues within regular secondary structure elements in the N-terminal domain of MBP (Sharff et al., 1993) (Figure 4) and in HCA II (Hakansson et al., 1992) (Figure 5). X-ray diffraction studies of MBP have established that the protein comprises two domains with the angle between the domains critically dependent on the bound sugar (Sharff et al., 1992). This suggests that the hinge region joining the domains may well be quite plastic and we have thus calculated separate alignment frames for each element. Somewhat different Euler angles describing the orientation of the alignment frames in the PDB X-ray frame have been obtained [(α,β,γ) = (104°, 28°, 31°), (78°, 31°, 50°), for the N- and C-terminal domains], indicating that the domains may be oriented somewhat differently in solution and crystalline states. Pairwise differences between measured (D^{meas}) and predicted (D^{pred}) dipolar couplings, $\chi_{rms} = [\{\sum_N (D^{meas} - D^{pred})^2/N\}^{0.5}]$, are reported for each type of coupling measured. Because the value of χ_{rms} is critically dependent on the degree of alignment, it is convenient to describe the level of agreement between a structural model and experimental parameters in terms of the quality factor, Q, defined by Bax and co-workers as, $Q = \chi_{rms} / D_{rms}$, where D_{rms} is the root-mean-squared value of D_{ij} calculated from the fitted axial and rhombic alignment values, on the assumption of an isotropic distribution of bond vectors (Ottiger and Bax, 1999). Q values for each type of dipolar coupling are listed in Figures 4 and 5 as well.

Conclusions

In summary, pulse schemes for the measurement of backbone dipolar couplings in high molecular weight proteins are presented which make use of recently developed TROSY methodology. The resolution provided by the 3D experiments facilitates the measurement of large numbers of couplings in high molecular weight protein systems. The dipolar couplings obtained from the present experiments serve as important additional structural restraints to the methyl-methyl, methyl-NH and NH-NH NOEs available from methyl protonated, ^{15}N,^{13}C,^{2}H-labeled proteins.

Acknowledgements

This research was supported by a grant from the Medical Research Council of Canada (L.E.K.). L.E.K. is an international Howard Hughes Research Scholar. The authors are grateful to Dr. Logan Donaldson for help with the production of phage and Dr. Nikolai R. Skrynnikov for helping writing the program used to calculate the orientation of the alignment frame and alignment parameters from measured dipolar couplings. The authors thank Professor Art Pardi and Mark Hansen (University of Colorado) for sharing the protocol for phage production prior to publication and for providing the lab with an initial phage sample.

References

Bodenhausen, G. and Ernst, R.R. (1981) *J. Magn. Reson.*, **45**, 367–373.

Boyd, J. and Scoffe, N. (1989) *J. Magn. Reson.*, **85**, 406–413.

Delaglio, F., Grzesiek, S., Vuister, G.W., Zhu, G., Pfeifer, J. and Bax, A. (1995) *J. Biomol. NMR*, **6**, 277–293.

Delaglio, F., Torchia, D.A. and Bax, A. (1991) *J. Biomol. NMR*, **1**, 439–446.

Emsley, L. and Bodenhausen, G. (1987) *Chem. Phys. Lett.*, **165**, 469–476.

Gardner, K.H. and Kay, L.E. (1998) *Annu. Rev. Biophys. Biomol. Struct.*, **27**, 357–406.

Gardner, K.H., Zhang, X., Gehring, K. and Kay, L.E. (1998) *J. Am. Chem. Soc.*, **120**, 11738–11748.

Garrett, D.S., Powers, R., Gronenborn, A.M. and Clore, G.M. (1991) *J. Magn. Reson.*, **95**, 214–220.

Geen, H. and Freeman, R. (1991) *J. Magn. Reson.*, **93**, 93–141.

Griesinger, C., Sørensen, O.W. and Ernst, R.R. (1986) *J. Chem. Phys.*, **85**, 6387–6852.

Hakansson, K., Carlsson, M., Svensson, L.A. and Liljas, A. (1992) *J. Mol. Biol.*, **227**, 1192–1204.

Hansen, M.R., Mueller, L. and Pardi, A. (1998) *Nat. Struct. Biol.*, **5**, 1065–1074.

Kay, L.E., Ikura, M., Tschudin, R. and Bax, A. (1990) *J. Magn. Reson.*, **89**, 496–514.

Kay, L.E., Keifer, P. and Saarinen, T. (1992) *J. Am. Chem. Soc.*, **114**, 10663–10665.

Marion, D., Ikura, M., Tschudin, R. and Bax, A. (1989) *J. Magn. Reson.*, **85**, 393–399.

Ottiger, M. and Bax, A. (1998) *J. Am. Chem. Soc.*, **120**, 12334–12341.

Ottiger, M. and Bax, A. (1999) *J. Biomol. NMR*, **13**, 187–191.

Ottiger, M., Delaglio, F. and Bax, A. (1998) *J. Magn. Reson.*, **131**, 373–378.

Patt, S.L. (1992) *J. Magn. Reson.*, **96**, 94–102.

Pervushin, K., Riek, R., Wider, G. and Wüthrich, K. (1997) *Proc. Natl. Acad. Sci. USA*, **94**, 12366–12371.

Pervushin, K., Riek, R., Wider, G. and Wüthrich, K. (1998a) *J. Am. Chem. Soc.*, **120**, 6394–6400.

Pervushin, K.V., Wider, G. and Wüthrich, K. (1998b) *J. Biomol. NMR*, **12**, 345–348.

Schleucher, J., Sattler, M. and Griesinger, C. (1993) *Angew. Chem. Int. Ed. Engl.*, **32**, 1489–1491.

Sharff, A.J., Rodseth, L.E. and Quiocho, F.A. (1993) *Biochemistry*, **32**, 10553–10559.

Sharff, A.J., Rodseth, L.E., Spurlino, J.C. and Quiocho, F.A. (1992) *Biochemistry*, **31**, 10657–10663.

Tjandra, N. and Bax, A. (1997) *Science*, **278**, 1111–1114.

Tjandra, N., Omichinski, J.G., Gronenborn, A.M., Clore, G.M. and Bax, A. (1997) *Nature Struct. Biol.*, **4**, 732–738.

Tolman, J.R., Flanagan, J.M., Kennedy, M.A. and Prestegard, J.H. (1997) *Nat. Struct. Biol.*, **4**, 292–297.

Venters, R.A., Farmer, B.T., Fierke, C.A. and Spicer, L.D. (1996) *J. Mol. Biol.*, **264**, 1101–1116.

Wang, Y.X., Marquardt, J.L., Wingfield, P., Stahl, S.J., Lee-Huang, S., Torchia, D.A. and Bax, A. (1998) *J. Am. Chem. Soc.*, **120**, 7385–7386.

Wishart, D.S. and Sykes, B.D. (1994) *J. Biomol. NMR*, **4**, 171–180.

Yang, D. and Kay, L.E. (1999a) *J. Biomol. NMR*, **13**, 3–9.

Yang, D. and Kay, L.E. (1999b) *J. Am. Chem. Soc.*, **121**, 2571–2575.

Yang, D. and Nagayama, K. (1996) *J. Magn. Reson.*, **A118**, 117–121.

Zhu, G. and Bax, A. (1990) *J. Magn. Reson.*, **90**, 405–410.

Zhu, G. and Bax, A. (1992) *J. Magn. Reson.*, **98**, 192–199.

Zhu, G., Kong, X.M. and Sze, K.H. (1999) *J. Biomol. NMR*, **13**, 77–81.

Zwahlen, C., Gardner, K.H., Sarma, S.P., Horita, D.A., Byrd, R.A. and Kay, L.E. (1998a) *J. Am. Chem. Soc.*, **120**, 7617–7625.

Zwahlen, C., Vincent, S.J.F., Gardner, K.H. and Kay, L.E. (1998b) *J. Am. Chem. Soc.*, **120**, 4825–4831.